

Mass-spectrometric mining of Hadean zircons by automated SHRIMP multi-collector and single-collector U/Pb zircon age dating: The first 100,000 grains

Peter Holden^{a,*}, Peter Lanc^a, Trevor R. Ireland^a, T. Mark Harrison^{a,b}, John J. Foster^a, Zane Bruce^a

^a Research School of Earth Sciences, The Australian National University, Canberra, ACT 0200, Australia

^b Institute of Geophysics and Planetary Physics, UCLA, Los Angeles, CA 90095-156, USA

ARTICLE INFO

Article history:

Received 29 October 2008

Received in revised form 12 June 2009

Accepted 12 June 2009

Available online 21 June 2009

Keywords:

SHRIMP

SIMS

Ion microprobe

Multi-collector

Geochronology

ABSTRACT

The identification and retrieval of a large population of ancient zircons (>4 Ga; Hadean) is of utmost priority if models of the early evolution of Earth are to be rigorously tested. We have developed a rapid and accurate U–Pb zircon age determination protocol utilizing a fully automated multi-collector ion microprobe, the ANU SHRIMP II, to screen and date these zircons. Unattended data acquisition relies on the calibration of a digitized sample map to the Sensitive High Resolution Ion MicroProbe (SHRIMP) sample-stage co-ordinate system. High precision positioning of individual grains can be produced through optical image processing of a specified mount location. The focal position of the mount can be optimized through a correlation between secondary-ion steering and the spot position on the target. For the Hadean zircon project, sample mounts are photographed and sample locations (normally grain centers) are determined off-line. The sample is loaded, reference points calibrated, and the target positions are then visited sequentially. In SHRIMP II multiple-collector mode, zircons are initially screened (ca. 5 s data acquisition) through their ²⁰⁴Pb corrected ²⁰⁷Pb/²⁰⁶Pb ratio; suitable candidates are then analyzed in a longer routine to obtain better measurement statistics, U/Pb, and concentration data. In SHRIMP I and SHRIMP RG, we have incorporated the automated analysis protocol to single-collector measurements. These routines have been used to analyze over 100,000 zircons from the Jack Hills quartzite. Of these, ca. 7%, have an age greater than 3.8 Ga, the oldest grain being 4372 ± 6 Ma (2σ), and this age is part of a group of analyses around 4350 Ma which we interpret as the age when continental crust first began to coalesce in this region. In multi-collector mode, the analytical time taken for a single mount with 400 zircons is approximately 6 h; whereas in single-collector mode, the analytical time is ca. 17 h. With this productivity, we can produce significant numbers of zircons for statistically limited studies including correlations between age and morphology, mineral-inclusion paragenesis, as well as isotopic studies including Hf and O isotopic compositions, Pu–Xe, and Sm–Nd isotopes.

© 2009 Elsevier B.V. All rights reserved.

1. Introduction

The identification of ancient detrital zircons from the Mt Narryer and Jack Hills localities (Western Australia) was one of the early successes of the Sensitive High Resolution Ion MicroProbe (SHRIMP) pushing back the oldest remnants of the early Earth to 4.2 Ga [1,2]. The abundance of 4 Ga zircons in these sedimentary rocks is low, only several percent, and even with an ion microprobe, the identification of them was painstaking. These old grains remain our only solid representatives of the earliest portion of Earth history. After their initial discovery, which was not without controversy [3,4], interest waned because analytical techniques at the micro scale

were still in their infancy. With the subsequent development of multi-collector ICPMS, and improved ion-probe measurements of stable isotopes, interest in the Hadean has been re-kindled.

The earliest portion of Earth history, the Hadean (4.5–4.0 Ga), is classically represented as a period of intense meteorite bombardment, high heat flow, and rapid geological recycling [5]. The proposed origin of the moon via the collision of the Earth with a Mars-sized body reinforces the view that the earliest part of Earth history must have been “hellish”. Cratering densities on the Moon, the lack of a terrestrial rock record, and thermal models all point to hot, energetic surface conditions.

Although the rock record presently extends back only as far as 4.0 Ga [6], individual mineral grains as old as 4.4 Ga can be recovered from early Archean meta-conglomerates in the Mt Narryer and Jack Hills locations in Western Australia [7]. From those few Hadean zircon samples, trace-element abundances and mineral inclusions

* Corresponding author. Tel.: +61 2 6125 0837; fax: +61 2 6125 0941.

E-mail address: Peter.Holden@anu.edu.au (P. Holden).

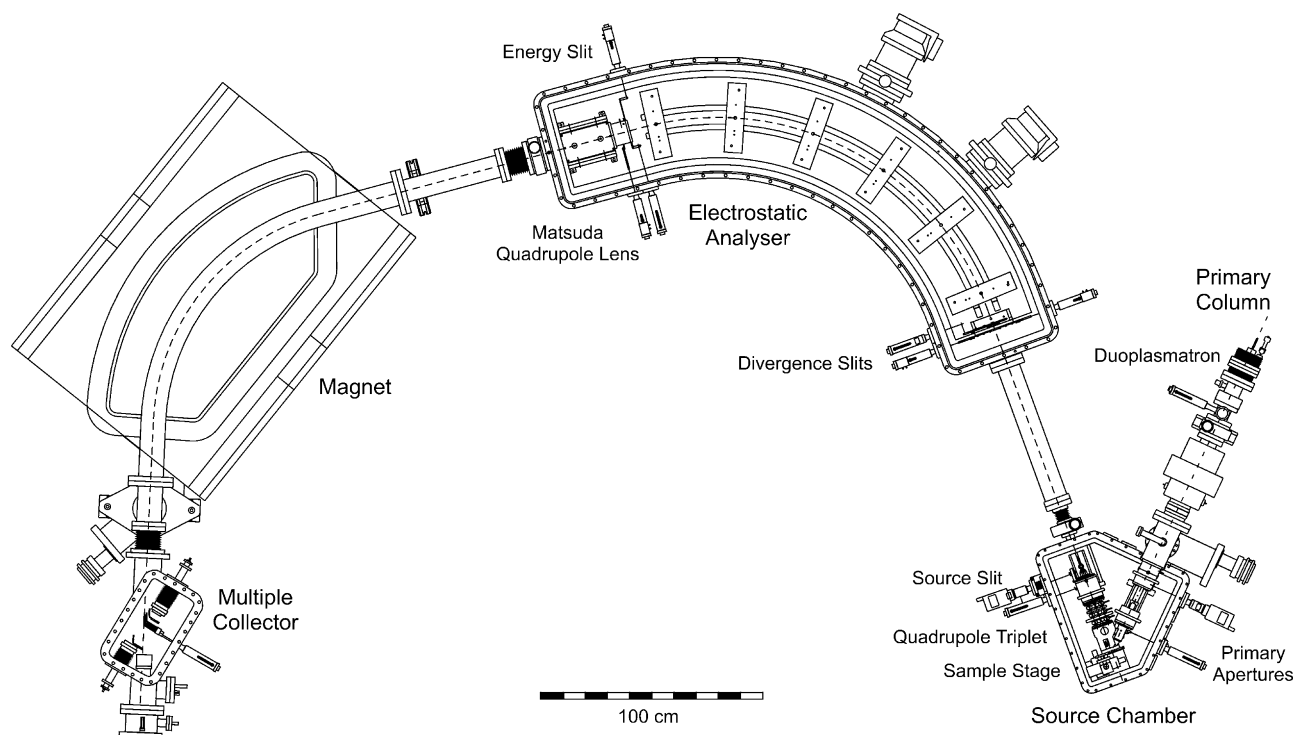


Fig. 1. Overall schematic of the ANU SHRIMP II.

suggested that the oldest zircons had formed under conditions no different than our recent geological past [8,9]. Moreover, oxygen isotopes from these zircons [7,10] suggest the involvement of surface water, weathering, and sedimentation in the history of >4-Ga granite protoliths.

Studies prior to this initiative have been based on only a few tens of Hadean zircons. With such small numbers of grains, it is difficult to adequately establish the proportions of different age populations, or establish potential geological relationships within the Hadean (e.g., presence of older inherited zircons as cores), or obtain a realistic characterization of the oldest populations of grains. In addition, our understanding of early Earth processes would be greatly enhanced if sufficient zircons could be recovered for isotopic analysis either as single grains, or in multi-grain samples [11]. Samples are needed to further investigate such fundamental questions as the timing of the initiation of continental crust formation, the timing and evolution of the atmosphere, and indeed the earliest indications of life on Earth. For these studies we estimate we need to analyze 150,000–300,000 Jack Hill zircons to obtain sufficient numbers of the oldest grains for detailed study. Using conventional ion-probe protocols, such an endeavor would require 10 years continuous operation to achieve just the lower limit. Such a commitment to the exclusion of all other scientific endeavor is simply not feasible. Moreover, prior to this initiative all SHRIMP determinations were carried out manually. With a minimum of 150,000 zircons to sift through, some form of automation is required. Herein we describe the techniques and developments that are being used using to efficiently find sufficient old zircons necessary for further investigations.

2. Methods

2.1. Instrumentation

The analytical protocols described below require an understanding of the physical layout of SHRIMP II and so an overview

is presented here (Fig. 1). The SHRIMP II multiple collector is described in detail for the first time.

The primary-ion source for zircon U–Pb analysis is a duoplasmatron producing O^- and O_2^- ions. The primary-ion beam is accelerated to near target potential (+10 kV) with selection of oxygen species (typically O_2^-) made with a Wien filter (velocity selection through orthogonal electrostatic and magnetic fields). The final spot image at the target is formed by demagnification (factor of approximately 7) of a selectable aperture that is located at the front focal point of the last lens (Kohler illumination). The incidence angle of 45° between the target and primary column yields elliptical spots on the target surface; a $100\ \mu\text{m}$ Kohler aperture will form a spot approximately $15 \times 20\ \mu\text{m}$.

One of the major features of SHRIMP is a confocal Schwarzschild optical system that allows target viewing during analysis. The optical system has a very shallow depth of field that requires very precise positioning ($<5\ \mu\text{m}$) in terms of the sample-stage X-drive. The optical focus is aligned with the ion-optical focusing such that the primary beam spot on the target is coincident with the center of the secondary extraction axis when the sample is in focus. Thus, simply bringing the target into optical focus also brings the target into the correct ion-optical alignment. This can be demonstrated by an optically focused image having a reproducible secondary-ion lateral steering (QT1Y; see Fig. 2 and text below) because the 45° incidence angle makes the lateral spot position covariant with focus. Conversely, the ion-optical steering can be used to optically focus the stage.

The positive secondary-ion beam is accelerated to (real) ground potential and transformed through a quadrupole triplet to produce an ion waist at the source slit thus maximizing transmission to the mass analyzer. The first lens of the triplet (QT1) is configured with each element having a separate power supply so that it has steering (QT1Y lateral, QT1Z vertical) as well as focusing capability.

The SHRIMP II mass analyzer (Fig. 1) is based on the ion-optical design of Matsuda [12] that features an astigmatic double-focusing mass spectrometer. The essential elements are a cylindrical elec-

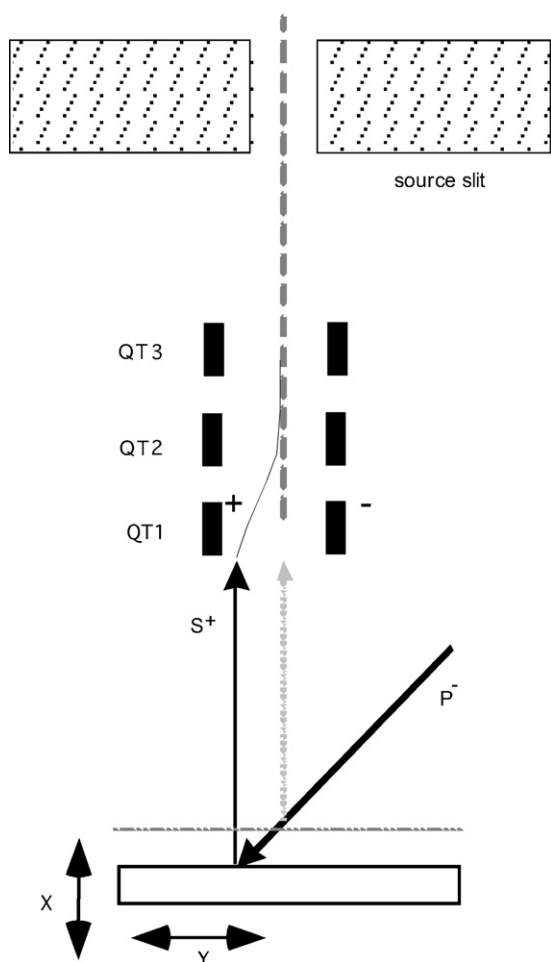


Fig. 2. Stage focusing using the secondary-ion optics. QT1–3 represent the three quadrupole stages of the main secondary-ion-optical element. Biasing the horizontal poles of the first element of the triplet (QT1Y) allows the secondary-ion beam (S^+) to be steered. X and Y represent the co-ordinate system with Z coming straight out of the page. Should the target be misplaced in the X direction (out of optical focus; see text) the travel path for the primary beam (P^-) will be shorter or longer than ideal, which in turn induces a lateral shift in the emission point of the secondary beam. Compensation for this error may be made by changing the QT1Y steering to maximize transmission through the source slit. Conversely, the difference between the observed QT1Y steering and the ideal can be converted into a physical distance in X for which the stage can be moved and the target brought back into focus.

trostatic analyzer (ESA; radius of 1.272 m), a sector magnet (radius of 1.000 m), and an electrostatic quadrupole lens positioned at the end of the ESA to reduce second order ion-optical aberrations.

The original SHRIMP II single-collector instrument has been modified to include a multiple collector (Fig. 3). The essential elements of the multiple collector are an axial array consisting of three ion counters that can be inserted into position at the central beam trajectory, two floating heads each with an ion counter and Faraday cup that can move along the focal plane (inclined at 28° relative to central-ray trajectory) on the high mass and low mass sides, respectively. A Faraday cup can alternatively be inserted in place of the axial array, or for operation in single-collector mode, an ion counter at the back of the multiple-collector chamber can be used when the axial array is retracted. The available configurations of these collectors (Table 1) are designed to maximize its capability in the analysis of light-mass stable isotopes (C, O, S), as well as Hf and Pb isotopes at high mass positions.

The axial array allows variable spacing so that it can be configured to allow unit mass collection for three masses between 180 and 210 amu approximately. The small absolute dispersion of the

Table 1
Acronyms for the SHRIMP II detector system.

	Channel
AAL	Axial Array Low mass ion counter
AAC	Axial Array Central-ray ion counter
AAH	Axial Array High mass ion counter
FHI	Floating head High mass Ion counter
FHF	Floating head High mass Faraday cup
FLI	Floating head Low mass Ion counter
FLF	Floating head Low mass Faraday cup
AFC	Axial Faraday Cup
AIC	Axial Ion Counter

Pb isotope peaks at the collector slits (3.4 mm), severely limits the space available and consequently the SHRIMP II multi-collector utilizes Sjuts™ (KBL 408) channel electron multipliers (CEM) that have a width of 5.0 mm. Conversion dynodes permit the CEM to be aligned normal to the focal plane, allowing them to be packed to the appropriate spacing. The mass resolution of the instrument may be changed by selecting one of the four collector slits via motorized movable slit bars, which, when combined with an adjustable source slit, allows the required mass resolution to be “dialed-in”. A single actuator moves the three axial array collector slit bars simultaneously so that the same position on each of the bar is selected. Following the slits, independently controlled (voltage) conversion dynodes focus secondary electrons on to the respective multipliers. The restricted spacing limits the axial array to an ion-counting capability only.

When the axial array is withdrawn, the central-ray beam can be collected in the axial Faraday cup (AFC), which is suspended and driven from the multi-collector lid, or, the beam can be passed back to an alternate axial ion-counting system (AIC) with an ETP™ discrete-dynode electron multiplier (DDEM) at the back of the chamber (Fig. 3). The divergence of the ion beam after the collector slit and the distance to the detector requires the use of a transfer lens (used in conjunction with a retardation lens) to refocus ions onto the AIC.

The two floating heads move along the focal plane from opposite sides of the central position. The low and high mass heads each have an independently controlled collector slit, a pulse-counting system (CEM) with externally controllable conversion dynode and electron multiplier accelerating potentials, as well as an insertable Faraday cup.

For zircon age determination the Pb isotopes plus $^{238}\text{U}^+$ and $^{238}\text{U}^{16}\text{O}^+$ are required. The axial array is inserted to collect $^{206}\text{Pb}^+$, $^{207}\text{Pb}^+$, and $^{208}\text{Pb}^+$, and the low mass head is brought in to collect the $^{204}\text{Pb}^+$ mass position (Fig. 4). The high mass floating head is positioned so that $^{238}\text{U}^{16}\text{O}^+$ is aligned when $^{238}\text{U}^+$ is collected in the same collector as $^{206}\text{Pb}^+$ (the axial array low mass collector; AAL). In this configuration, all Pb isotopes can be measured simultaneously, and with a single mass step, U^+ and UO^+ can be determined as well.

An $80\ \mu\text{m}$ source slit and $100\ \mu\text{m}$ collector slits in the axial array produce a 1% valley resolution of greater than 5000, sufficient to completely resolve REE and HfSi interferences from the Pb isotope peaks ($<0.01\%$). The limited resolution required for $^{238}\text{U}^{16}\text{O}^+$ means a wider collector slit can be used (ca. $300\ \mu\text{m}$) that produces more flat on the top of the peak and allows some flexibility in tuning and positioning.

2.2. Data acquisition

The accurate measurement of Pb isotope ratios on beam sizes of 400 kHz and below requires an ion pulse-counting system. While the sensitivity of electron multipliers is their major advantage, they have several disadvantages such as dead-time and gain drift. In

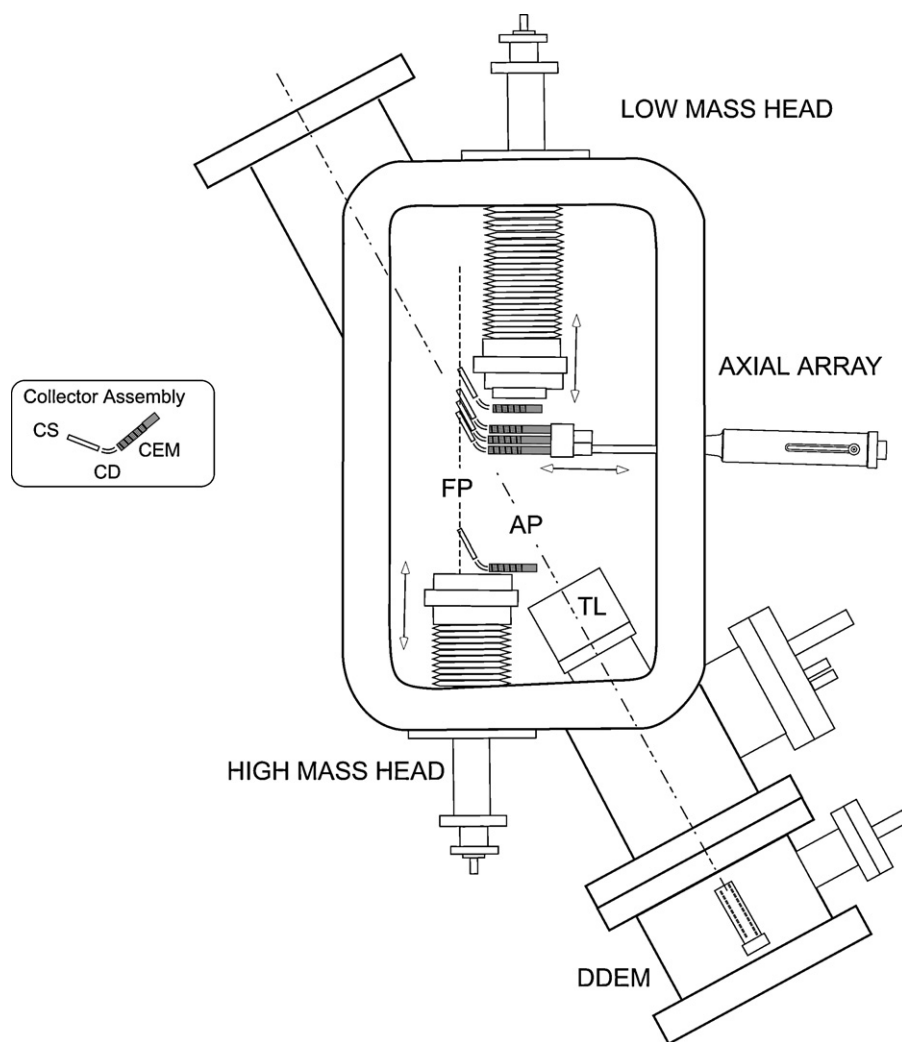


Fig. 3. Schematic layout of SHRIMP II multi-collector. FP is the magnet focal plane, AP is the plane of the axial beam trajectory, TL is the transfer lens, CS is the collector slit, CD is the conversion dynode, CEM; channel electron multiplier, DDEM; discrete-dynode electron multiplier. The low and high mass floating heads are extendable along the FP. The collector assembly inset shows an expanded view of the relationship between the CS, CD and CEM.

single-collector mode, gain drift affects all ion beams in a similar fashion and so it is normalized out in the determination of isotope ratios. However, in multiple-collector mode, each channel may behave differently and so the effects of drift must be monitored. This is particularly the case for CEM which have a much shorter life expectancy (approximately 10^{10} counts) compared to the ETP™ DDEM (10^{13} – 10^{14} counts).

The effect of gain changing for an individual CEM is illustrated in Fig. 5 for Si isotope measurements on Si metal. Each datum represents 10 blocks of 10 scans with an integration period of 20 s (further subdivided into 10 units of 2 s). The slope in the $^{29}\text{Si}/^{28}\text{Si}$ and $^{30}\text{Si}/^{28}\text{Si}$ is entirely due to the aging (drift) in the low mass CEM, because of the relatively high count rate for $^{28}\text{Si}^+$ of 200 kHz. Since the gain drift is so uniform, we can calculate the drift at approximately 2×10^{-10} per incident Si^+ ion. On the other hand, the $^{30}\text{Si}/^{29}\text{Si}$ ratio (Fig. 5b) stays constant over the 30-min period indicating that the rate of drift is acceptable at low (<20 kHz) count rates. For Pb isotope measurements at count rates of ca. 10 kHz, the CEM drift characteristics are quite satisfactory.

The stability of CEM operation is primarily established through the high voltage applied across the CEM. A typical CEM gain curve is shown in Fig. 6 showing the relatively flat response for voltage above 2.2 kV. Each SHRIMP ion-counter channel is handled by a discrete pulse-counting system incorporating the conversion dyn-

ode voltage, the discriminator potential, and the voltage to the CEM controlling amplification. The CEM have dark noise in the order of 0.2 counts per minute and this is negligible for measurements of old zircons.

3. Analytical protocols

3.1. Sample preparation

The Jack Hills zircon grains are mounted in a grid pattern to facilitate sample documentation and subsequent retrieval from the mount. Initially mounts incorporated a 10×10 matrix but 20×20 grids allow more grains to be analyzed in a session and so these are now used exclusively. Standard zircons (AS3) are typically positioned outside the matrix (Fig. 7). The main restriction in the mount preparation is to avoid getting too close to the edge of the 25 mm steel mount holders, which can cause perturbations in the ion extraction field and thereby affect U–Pb calibrations.

For zircon geochronology, grains are typically polished to mid-section, imaged in reflected and transmitted light, and then imaged by cathodoluminescence in an electron microscope. However, the issue with the zircon mining is to recover the largest possible mass of old zircon and so only a minimal polish is applied. Furthermore, with a rejection rate of 93%, such detailed documentation is extrav-

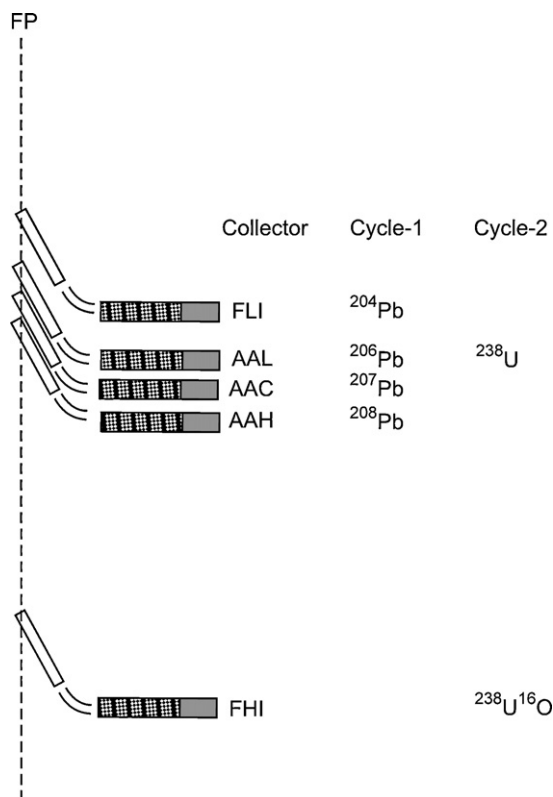


Fig. 4. Multiple-collector setup for U–Pb age determination in zircon. Collector names as in Table 1, FP is the magnet focal plane. Only one mass jump is required to measure all the U and Pb isotopes necessary for age dating.

agent for every zircon in the mount. Given the shallow probe pit generated during this type of analysis (less than 1 μm), imaging of the selected Hadean grains is carried out after the age characterization.

The only image required prior to analysis is a reflected-light map of the whole mount. The conventional method of producing this map is to stitch together low magnification reflected-light petrological microscope images. However, image distortion (geometrical) and stitching errors make this an unsatisfactory method, since automated analyses require an accurate cross-calibration between grain locations on the map, and stage locations inside the SHRIMP source. Presently we use a stereoscopic microscope with coaxial illumination that can take a single reflected-light image of the whole mount.

3.2. Sample locations

For automated analysis, a predefined series of analytical points must be generated. This can be accomplished in two ways – either by visiting the desired locations in the SHRIMP and saving their locations, or by generating a list of sample locations off-line. For a sample mount with 400 grains awaiting analysis, it would be no small task to visit each point and register its position. Moreover, uninterrupted driving of the in-vacuum sample-stage motors can cause progressive errors in the positioning that can then compromise the unattended analysis. It is therefore imperative that spot locations be assigned outside the ion probe so that all grains are fixed in an absolute reference framework.

The required analytical locations are marked up on the digital image of the sample mount via an in-house LabView™ software package (GPIX), and the positions are recorded in Cartesian (pixel) co-ordinates. The pixel map and its accompanying sample co-ordinate list are then loaded into the SHRIMP Sample Stage soft-

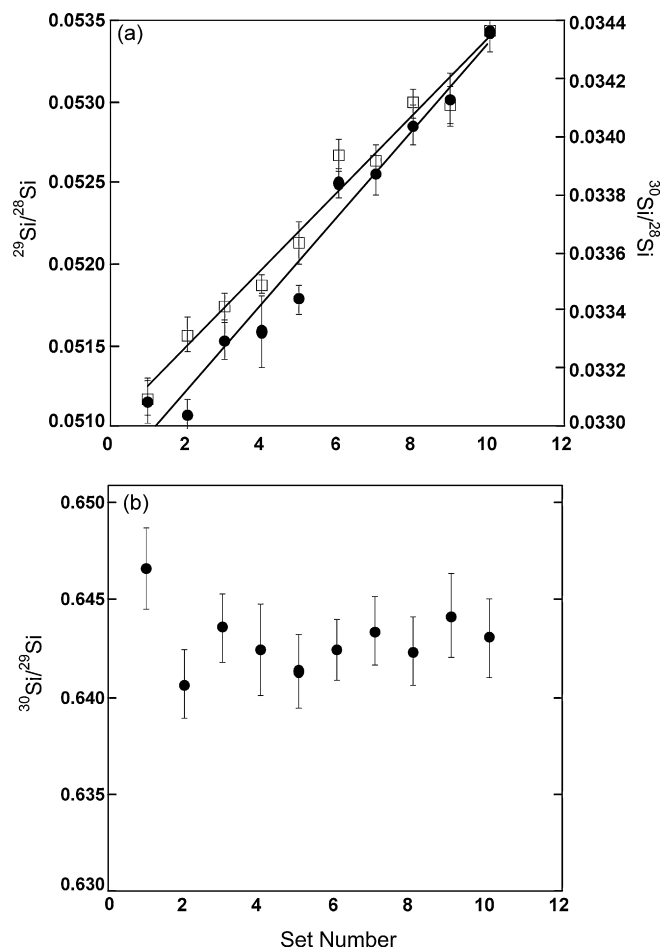


Fig. 5. (a) The change in Si isotope ratios measured on three CEM's as a function of time. Each set consists of 20 ratios of 10-s integrations. The lines are linear regressions through each data set. The very linear drift in both ratios is a function of the “ageing” of the FLI CEM detector ($^{28}\text{Si}^+$) at relatively high (200 kHz) count rates. (b) The ratio of $^{30}\text{Si}^+ / ^{29}\text{Si}^+$ measured as a function of time. At lower count rates ($^{29}\text{Si}^+ = 10$ kHz) this ratio did not drift appreciably over the 30 or so minutes of data acquisition.

ware. With the sample in the source chamber, four registration points on the mount are visited and their positions logged. Then the pixel co-ordinates of the spot locations can be converted using a projective transformation to the sample stage co-ordinates (Pixel Interpolated Mapping System, PIMS). The sample-stage locations

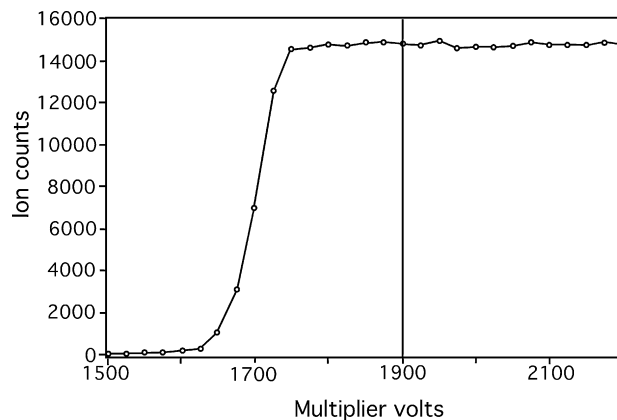


Fig. 6. A typical CEM gain curve in this case for the AAC collector. All five curves were similar, and for U–Pb analyses values of 1900 ± 50 V (represented by the vertical line) were chosen.



Fig. 7. Zircons mounted in a 20×20 grid pattern. The “way-up” registration arrow on the back of the mount allows each grain to be identified and extracted for further analysis.

are specified in terms of X – Y – Z (X =focal position, Y =horizontal position, Z =vertical position) whereas the pixel map is only specified in two dimensions. Thus, any tilt resulting in differential focus can be corrected.

One grain, usually close to the center of the mount, is used as a further reference point. A video image of this grain is stored so that the location can be periodically revisited (regularity defined by the user) for a pattern match from which any stage drift can be determined. The pattern matching typically positions the sample within 1 bit (ca. $3 \mu\text{m}$) in terms of Y - and Z -axis co-ordinates.

PIMS achieves only a coarse calibration of focus over the mount because of the small number of registration points. A focusing method involving a fast Fourier-Transform histogram of the image has been trialed, but the method is relatively slow and is subject to error especially when scratches are present. Provided PIMS gets the target close to position, the correlation between spot position and SHRIMP secondary-ion-optic steering can be used to achieve an accurate optical focus. As indicated above, there is a direct correlation between the “ X ” focal position (in–out) and the horizontal “ Y ” position (Fig. 2). Undulation or tilting of the sample surface, which can affect the optical focus, will cause a concomitant shift in “ Y ” steering. By scanning the horizontal component of the first element of the quadrupole triplet (QT1Y), the measured maximum can be compared to an in-focus reference value and a deviation calculated. This is converted into an X -axis stage-drive offset to bring the target into optical focus and the primary beam back to the ion-optical center.

3.3. Automated analysis

Once the PIMS setup has been completed and the accuracy of a few test points assessed, the sample can be analyzed unattended. The analytical routine involves visiting the reference point to maintain accurate positioning, analyzing zircon U–Pb standards, and analyzing the detrital zircons.

For the reference point, the focus is checked with a scan of the QT1Y steering, and the current image compared to the reference image for YZ location, and any offset recorded for addition to sub-

sequent recorded positions. For the standard and detrital zircons, the stage is moved to the specified XYZ position (including any offset previously calculated), the focus checked with the QT1Y steering, and then the analytical routine is started. Upon completion of the age determination, the stage is moved to the next zircon in the list. It is worth stating at this point, that these automated protocols work equally well for single-collector mode, in this instance the secondary beam being cycled quickly through ^{206}Pb and ^{207}Pb to estimate the age.

For unattended analysis, protocols must be established for conditions that jeopardize the run. Some conditions are non-fatal, such as the absence of a secondary beam from a grain that is not zircon, while other conditions necessarily terminate the session, such as the dropping-out of the source duoplasmatron arc discharge. We have found the most common issue with automatic analysis to be the progressive deterioration of the sample-stage positioning causing the primary beam to eventually miss a sample. This deterioration is generally the result of loss of steps in the stepper motors, although stage backlash can be an issue. Both of these effects can be minimized, though not removed, through appropriate choice of stage control parameters (acceleration, maximum speed), and regular servicing of the stage bearings (annual).

However, in the event that a grain is missed, and no secondary beam can be detected, the system initiates the Hunt mode. The “failed” location is used as the center of a square $100 \mu\text{m}$ on a side and the stage drives sequentially to the eight locations on the corners and midpoints of the sides. After a wait period of 1 s to burn through the gold coating, a 0.5 s integration is taken of the Zr_2O^+ (single-collector mode) or $^{206}\text{Pb}^+$ (multiple-collector mode). The software then drives the stage to the position with the highest count rate and the analysis resumes. A “snap” image (from the SHRIMP optical microscope) can be used to verify the spot location. Here the sample grid pattern also helps, we have not yet seen the wrong zircon analyzed because each grain is relatively far apart. If the Hunt mode fails to find a suitable analytical site, the stage drives to home to reset the positioning system, and then tries again. Three failures will cause the analysis routine to abort.

3.4. Zircon age measurement

Measurement details for zircon age dating by SHRIMP in single-collector mode have been covered in detail previously [13]. The $^{206}\text{Pb}/^{238}\text{U}$ age of an unknown is determined through calibration against a standard zircon of known age. A log plot of $^{206}\text{Pb}/^{238}\text{U}$ versus $^{254}\text{UO}/^{238}\text{U}$ typically conforms to a power-law fit (Fig. 8). The age of the unknown is calculated from the ratio of the unknown $^{206}\text{Pb}^+/^{238}\text{U}^+$ ratio to that ratio measured in the standard at a common $^{238}\text{U}^{16}\text{O}^+/^{238}\text{U}^+$ value (Eq. (3); see below).

For Hadean zircon analysis, there are two issues. First, we want to identify potentially old zircons as quickly as possible; for this reconnaissance mode, we only need $^{207}\text{Pb}/^{206}\text{Pb}$ ages. Secondly, for those potentially old zircons identified, we want to know some more details such as U and Pb concentrations and concordance. Initially, these two measurements were done separately with the sample mounts being reloaded after reconnaissance identification for more accurate single-collector measurement. However, the reliability of the multiple collection system makes this double handling unnecessary. The two separate analytical regimes, reconnaissance surveying and geochronology can be combined by using the rapid $^{207}\text{Pb}/^{206}\text{Pb}$ ratio as a screen to be followed by a protocol that reproduces the data obtained from single-collector acquisition as much as possible.

In reconnaissance mode, Pb isotope ratios are monitored immediately the beam is turned on. If after penetrating the Au coat, the $^{207}\text{Pb}/^{206}\text{Pb}$ stays above 0.4, the grain is potentially old and an extended routine is started including rastering of the primary beam,

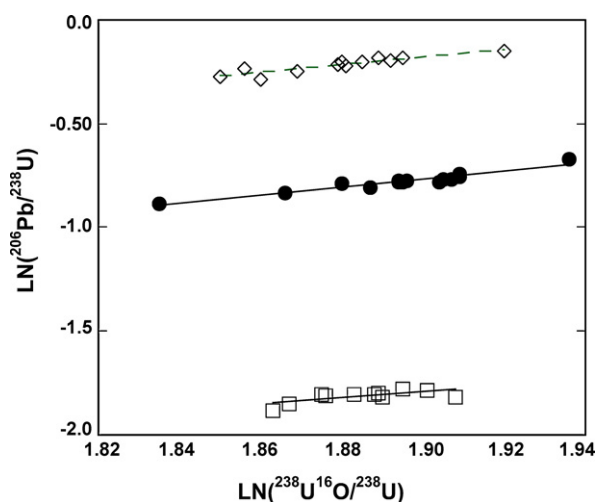


Fig. 8. Plot of $\ln(^{206}\text{Pb}/^{238}\text{U})$ versus $\ln(^{238}\text{U}^{16}\text{O}/^{238}\text{U})$ for standard zircons Temora (\square) [18], FC1 (\bullet) [16], and QGNG (\diamond) [18]. The $^{206}\text{Pb}/^{238}\text{U}$ ratio (and hence age; Eqs. (3) and (4)) is extracted via the offset between the standards and unknowns (Eq. (2)). Results for this run are given in Table 2.

tuning, and a full U–Pb determination. A reconnaissance analysis can last as little as 5 s.

A typical single-collector run incorporates 9 mass stations and 7 cycles of data acquisition and takes up to 20 min to complete. Of the nine mass stations used in single collection mode, six are directly relevant to the determination of the Pb–Pb and U–Pb ages (Eqs. (1)–(4)). Since the objective is to streamline the age determination process, these mass stations can be divided into the multi-collection of the Pb peaks ($^{204}\text{Pb}^+$, $^{206}\text{Pb}^+$, $^{207}\text{Pb}^+$), followed by the multi-collection of $^{238}\text{U}^+$ and $^{238}\text{U}^{16}\text{O}^+$ (Fig. 4). Single-collector measurements also determine Zr_2O^+ , $^{208}\text{Pb}^+$, and $^{232}\text{Th}^{16}\text{O}^+$. The $^{238}\text{U}^+/\text{Zr}_2\text{O}^+$ ratio is used for the determination of the U concentration. In multiple-collection mode, we can use the $^{238}\text{U}^+$ signal relative to the concurrent total secondary-ion beam as a proxy for U concentration. We can also calculate the Th/U and Th concentration from the $^{208}\text{Pb}/^{206}\text{Pb}$ coupled with the apparent age from the $^{207}\text{Pb}/^{206}\text{Pb}$ measurement. Baselines are gathered during the raster period rather than being an explicit mass step with the resulting benefit that the acquisition cycle contains only one mass jump, switching between $^{206}\text{Pb}^+$ and $^{238}\text{U}^+$ in the AAL detector.

$$\left(\frac{^{207}\text{Pb}}{^{206}\text{Pb}}\right)_m = \frac{1}{137.88} \frac{(e^{\lambda_{235}t} - 1) G_{\text{AAL}}}{(e^{\lambda_{238}t} - 1) G_{\text{AAC}}} \quad (1)$$

$$\left(\frac{^{206}\text{Pb}}{^{238}\text{U}}\right)_m = \frac{(^{206}\text{Pb}^+ / ^{238}\text{U}^+)_{\text{std}} ((^{206}\text{Pb}^+ / ^{238}\text{U}^+) (G_{\text{AAL}} / G_{\text{AAL}}))}{a((^{238}\text{U}^{16}\text{O}^+ / ^{238}\text{U}^+) (G_{\text{FHI}} / G_{\text{AAL}}))^2} \quad (2)$$

$$\left(\frac{^{206}\text{Pb}}{^{238}\text{U}}\right)_m = (e^{\lambda_{238}t} - 1) \quad (3)$$

$$t = \frac{\ln(^{206}\text{Pb}/^{238}\text{U})_m}{\lambda_{238}} \quad (4)$$

For Eqs. (1)–(4), the subscript m denotes the measured ratio, G subscript AAC, AAL and FHI are the measured gain factors for the respective multipliers (Table 1), λ_{235} and λ_{238} are the decay constants for ^{235}U and ^{238}U , respectively, and a is the calibration value of the day as measured on the standard. The Pb–Pb ages were determined using Eq. (1) and the $^{206}\text{Pb}/^{238}\text{U}$ ratio against a calibration standard zircon ($^{206}\text{Pb}/^{238}\text{U}_{\text{std}}$) using Eq. (2). The relationship between $^{206}\text{Pb}/^{238}\text{U}$ and age is given in Eqs. (3) and (4).

3.5. Gain calibration

Eqs. (1) and (2) show that the relative gain of each collector must be well calibrated if high accuracy isotope ratios are to be obtained. The arrangement of the peaks in the analytical cycle is designed to minimize the amount of post-analysis gain drift correction. The $^{206}\text{Pb}^+$ and $^{238}\text{U}^+$ are measured in the same CEM following the mass jump and so this ratio is unaffected by gain drift in the AAL CEM (Eq. (2)). Consequently, drift in the measured $^{206}\text{Pb}/^{238}\text{U}$ ratio over the analytical session is solely dependent on the relative gain change between the AAL ($^{238}\text{U}^+$) and FHI ($^{238}\text{U}^{16}\text{O}^+$) CEM.

Based on the results of the Si isotope analysis (outlined above), significant gain drifts on an hourly timescale are only detectable when count rates exceed 20 kHz. Typically, zircons from Jack Hills have low U contents (high U grains simply do not survive) and $^{206}\text{Pb}^+$ and $^{238}\text{U}^+$ seldom exceed 10 kHz, whereas $^{238}\text{U}^{16}\text{O}^+$ would be in the 20–50 kHz range. Therefore, a progressive change in calibration is to be expected through the drift in gain of the FHI relative to the AAL detectors. The relative gain between these collectors can be treated simply as a temporal calibration shift based on the analysis of the standards. In practice however, stepping $^{238}\text{U}^{16}\text{O}^+$ into the AAL and FHI channels at the start and end of the analytical session simplifies computing the gain drift.

While the $^{207}\text{Pb}/^{206}\text{Pb}$ age is critically dependent on both the relative gain between AAC and AAL (Eq. (1)) and the amount of drift over the session, none of the mounts analyzed thus far has required a drift correction between these detectors. The relative gain between the two channels can be determined by measuring standards with known isotopic composition, such as common Pb-rich materials (e.g., Broken Hill Feldspar or NIST 610 glass). Gain drift is also monitored as a consequence of the analyses of the zircon standard AS3 used for the U–Pb calibration.

The $^{207}\text{Pb}/^{206}\text{Pb}$ age as well as being dependent on the gain and its stability, is also highly dependent on the common Pb correction (as is the case for single-collector data acquisition). Scattered ions within the collector chamber present a potentially serious problem for the common Pb correction particularly for younger materials with little ^{207}Pb . For example, for an AS3 standard (1099 Myr) with 200 cps $^{207}\text{Pb}^+$, a one count per second over-count at mass 204 is equivalent to subtracting 50 Ma from the uncorrected $^{207}\text{Pb}/^{206}\text{Pb}$ age. Measuring an accurate baseline therefore, is vital for accurate ages to be computed. While the dark noise for a Sjtus™ CEM is of the same order as that of the larger ETP™ DDEM, we observe about 0.3 cps more baseline counts for the CEM (in the axial array) than that seen in the AIC for the same mass position. We attribute these additional counts to reflected secondary ions, possibly related to heavy rare-earth-element molecules, or to stray electrons, which are not transmitted through the retardation lens to the AIC. Nonetheless, accurate ages are determined (see below) albeit with slightly expanded uncertainties, relative to our single-collector results, due to the propagation of errors from the larger baseline subtractions.

Following baseline and gain corrections, data are output to a format compatible with the SQUID/ISOPLOT data reduction package [14].

4. Results

4.1. Standards

Before embarking on the surveying of unknowns, a mount containing zircon standards FC1, QGNG, and Temora 2 [15], was analyzed on an overnight fully automated multi-collector session to verify functionality. The $^{206}\text{Pb}/^{238}\text{U}$ age for the standards shows a systematic drift from younger to older ages as the run progresses (Fig. 9a). This drift can be attributed to a measured change in

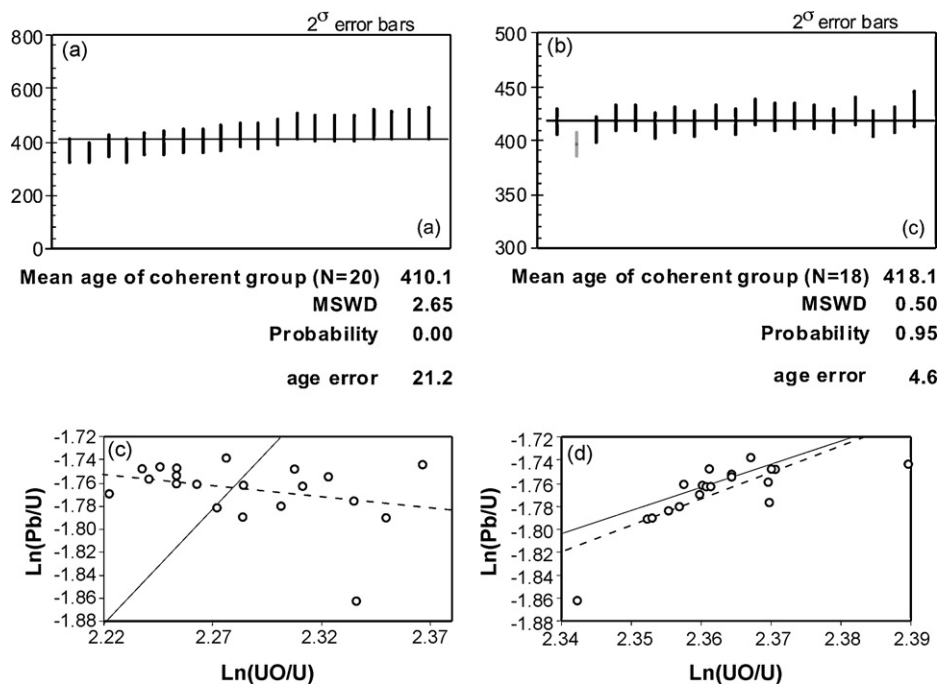


Fig. 9. (a) Apparent age of the Temora 2 standard with time of analysis during the session (output from SQUID [14]). The increasing apparent age is caused by the relative change in the gain of FHI ($^{238}\text{U}^{16}\text{O}^+$). (b) The expected slope 2 line is not observed (solid line). (c) Same data after a linear time interpolated gain drift correction of 10.0% had been applied to the FHI. (d) Predicted slope 2 line (Eq. (2); solid line) and best-fit regression through the data (dotted line) correspond.

the gain of 16.6% over the 18-h run period for the FHI collector ($^{238}\text{U}^{16}\text{O}^+$) relative to the AAL collector ($^{206}\text{Pb}^+$, $^{238}\text{U}^+$). This drift can be removed through a simple linear time interpolated drift correction (Fig. 9b). Variations in $^{206}\text{Pb}^+ / ^{238}\text{U}^+$ versus $^{238}\text{U}^{16}\text{O}^+ / ^{238}\text{U}^+$ before and after correction are shown for reference in Fig. 9c and d. The final corrected U–Pb and Pb–Pb ages are within error of published TIMS, and previous SHRIMP determinations (Table 2).

In order to check that the drift correction was appropriate for unknowns, we measured one mount (ANU 73) on SHRIMP II using the multi-collector data acquisition, and then re-measured the same spots on SHRIMP RG via standard single-collector protocols [13]. Table 3 shows a comparison of results after the application of the linear time interpolated drift correction for the multi-collector data, with those for the single-collector run. For standard AS3 on mount ANU 73 typical $^{207}\text{Pb}/^{206}\text{Pb}$ age errors for individual zircons ranged from 9.8 to 15.4 Ma for the single-collector run (SHRIMP RG), and from 16 to 44 Ma for the multi-collector run. The mean $^{207}\text{Pb}/^{206}\text{Pb}$ ages were within error of the true value in both cases (1095 ± 6 Ma and 1107 ± 20 Ma, respectively versus 1099 ± 1 Ma [16]). The integration times for the Pb^+ peaks were the same (30 s) for both runs and the higher errors in the multiple-collector run simply reflect the larger error uncertainty from the larger multi-collector baseline corrections. However, with the higher $^{207}\text{Pb}/^{206}\text{Pb}$ of the ancient grains, this effect is substantially de-magnified.

The two data sets of Jack Hills detrital grains are also presented in Table 3. In this case the larger $^{207}\text{Pb}/^{206}\text{Pb}$ age errors from the multiple-collector data are due to a shorter integration time for the Pb isotope peaks (5 s for multi-collector versus 10 s ^{206}Pb and 20 s

^{207}Pb single-collector). Likewise, multi-collector U–Pb ages are on average a factor of two less precise than the single-collector ages for the same reason.

The first order observation in comparing the two data sets is that zircons deemed concordant or near-concordant by multi-collector acquisition had this determination corroborated by the single-collector run, with the sole exception of ANU73-15.9, for which the single-collector U–Pb age was significantly lower, despite the $^{207}\text{Pb}/^{206}\text{Pb}$ ages agreeing within error. For the discordant grains, the multi-collector ^{204}Pb corrected U–Pb data shows systematically greater discordance than the single-collector data. This is difficult to reconcile as an analytical artifact since the $^{207}\text{Pb}/^{206}\text{Pb}$ ages generally agree and ^{204}Pb overcorrection can be ruled out. It is more likely that the effect is real and related to the multiple-collector data representing the outermost portion of the zircon that is indeed more discordant. Only two of the analyzed zircons have significantly different ^{204}Pb corrected $^{207}\text{Pb}/^{206}\text{Pb}$ ages between techniques, and in both cases (ANU73-3.1 and ANU73-5.11) expanded errors were due to large common Pb corrections. Again in both these cases, the subsequently obtained single-collector age was the older and less discordant (847% multi versus 336% single), perhaps supporting the notion that the outer portions of these grains have indeed suffered greater damage. This is to be expected, and it is worth re-stating that our over-arching objective is to recover the greatest possible mass of Hadean zircon, and for this reason and as outlined above, only a cursory polish is applied rather than polishing to midsection when the objective is accurate geochronology.

For the purposes of identifying ancient concordant zircons, the multi-collector data agrees closely with the single-collector data,

Table 2
Ages of standards QGNG [18] and FC1 [16] measured against Temora 2 (417 Ma [15]). Data reduced using the SQUID–ISOPLOT package [14].

	$^{204}\text{corr}$ $^{206}\text{Pb}/^{238}\text{U}$ age (Ma)	2σ error	$^{204}\text{corr}$ $^{207}\text{Pb}/^{206}\text{Pb}$ age (Ma)	2σ error	Concordia age (Ma)	2σ error
QGNG	1834	14.9	1849	3.6	Discordant	
FC1	1095	10.1	1096	3.6	1096.1	4.3

Table 3
Ages for the same analyzed spot on two different instruments SHRIMP II multi-collector and SHRIMP RG single-collector.

	Multi-collector				RG single-collector					
	$^{204}\text{Pb}/^{206}\text{Pb}/^{238}\text{U}$ age (Ma)	2 σ error	$^{204}\text{Pb}/^{207}\text{Pb}/^{206}\text{Pb}$ age (Ma)	2 σ error	%Discordant	$^{204}\text{Pb}/^{206}\text{Pb}/^{238}\text{U}$ age (Ma)	2 σ error	$^{204}\text{Pb}/^{207}\text{Pb}/^{206}\text{Pb}$ age (Ma)	2 σ error	%Discordant
ANU73-14	810	34	3310	42	309	1247	19	3304	20	165
ANU73-112	3980	137	3977	14	0	4036	52	3994	5	-1
ANU73-115	2953	108	4016	13	36	3640	48	4042	10	11
ANU73-31	569	86	3295	120	479	3011	45	3375	11	12
ANU73-4.1	2875	106	4005	15	39	3274	46	4001	6	22
ANU73-4.11	4033	141	3996	13	-1	4069	54	3981	6	-2
ANU73-4.15	2823	107	4140	16	47	3040	45	4107	8	35
ANU73-5.4	3641	132	3990	18	10	3335	49	3990	18	20
ANU73-5.11	407	18	3850	36	847	912	15	3972	16	336
ANU73-6.10	3998	138	4049	14	1	4029	55	4024	7	0
ANU73-8.14	4048	148	4012	18	-1	4031	61	3993	10	-1
ANU73-10.9	4173	157	4060	19	-3	3805	63	4050	21	6
ANU73-12.13	4030	137	4095	11	2	3701	52	4045	6	9
ANU73-14.8	3869	137	3926	28	1	3784	55	3930	8	4
ANU73-14.12	3984	176	4140	36	4	4091	96	4098	18	0
ANU73-15.6	3903	132	3903	14	0	3838	50	3889	6	1
ANU73-15.8	4021	149	4007	18	0	3893	62	4002	10	3
ANU73-15.9	3804	134	3969	16	4	3127	46	3974	8	27

while taking a third of the time. We therefore conclude that this technique is ideally suited to detrital zircon studies and especially to the recovery of Earth's oldest remnants.

4.2. The Jack Hills detrital population

The existence of a population of ancient detrital zircons from the Jack Hills and Mt Narryer regions is proof that continental crust formed as early as 4.35 Ga, and continued to form in this region after that. How these grains came to be incorporated into a 3.0 Ga meta-conglomerate and the extent of the Hadean ancient protolith at the time of sedimentation is less certain.

A probability histogram for 4500 Jack Hills zircons (maximum allowed by ISOPLOT) is shown in Fig. 10a. These zircons were analyzed with the rapid multi-collector protocol but without screening for $^{207}\text{Pb}/^{206}\text{Pb}$ at 0.4. The prominent maximum at ca. 3.4–3.5 Ga and the lesser maximum at 4.0–4.1 Ga are similar to previous results [2] and indicate an overall abundance of the >3.8 Ga zircons to be about 7%. Moreover, the data represents a variety of size fractions and we can find no discernable difference between the Hadean abundances in fine-grained and coarse-grained fractions. Thus, in the search for Hadean zircons for further isotopic work where a specific minimum mass of zircon is required, a greater mass-yield is obtained from the coarse-grained fractions.

Of the 103,150 grains that have now been screened, 7946 have ^{204}Pb corrected $^{207}\text{Pb}/^{206}\text{Pb}$ greater than 0.4 and thus have had U–Pb and Pb–Pb ages determined. Of these 7502 or 7.3% of the population were confirmed as being older than 3.8 Ga by the extended multiple-collector analysis. It should be noted however, that the 3.8–3.9 Ga population in Fig. 10b, is almost certainly under-represented because of the $^{207}\text{Pb}/^{206}\text{Pb}$ cut-off applied prior to full analysis at an age equivalent to 3940 Ma. From the 3.8–4.0 Ga population 1287 or 55.9% are within 10% of concordance; for the 4.0–4.2 Ga grouping 3347 of 4850 grains (69.0%) are similarly “concordant”. For the greater than 4.2 Ga group 213 of 349 (61.0%) are “concordant”, while 33 “concordant” grains out of 66 (50.0%) are older than 4.3 Ga. From all scanned grains, only 11 concordant and 9 discordant grains as old as or older than 4.35 Ga have been identified, representing 107 and 87 ppm of the total Jack Hills population, respectively. The oldest grains so far analyzed have Pb–Pb ages of 4372 ± 6 Ma and 4371 ± 12 (2σ) Ma and are slightly (2% and 5%) discordant. Not only are these the oldest ages, but they form the abrupt upper age limit to a population of 23 grains (weighted mean of 4344 ± 6 Ma) that represents the age maxima in the total population. This possibly represents the time at which continental crust first coalesced into stable platforms in this region.

We have found no further indications of zircon with $^{207}\text{Pb}/^{206}\text{Pb}$ ages as old as 4404 ± 8 Ma (2σ), which is the oldest age in the Jack Hills detrital population of Wilde et al. [7]. This age is present in a discrete outer zone of grain W74/2-36 while the remainder of the grain has a bimodal distribution of ages around 4350 and 4280 Ma ([7]; Table 1). The dominant age component of grain W74/2-36 has the same age as our upper cut-off and we believe that this grain was likely formed at ca. 4350 Ma. The 4404 Ma zone likely represents an area of localized Pb heterogeneity where the data reduction protocols utilized have resulted in an overestimate of the $^{207}\text{Pb}/^{206}\text{Pb}$ age.

The constantly increasing abundance of zircons from 4.3 to 4.1 Ga (for fully analyzed grains within 10% of concordance; Fig. 10b), suggests a flourishing of granitoid formation once the process had been initiated. Furthermore, the age data appears part of a continuum, rather than defining discrete episodic magmatic events. No age gaps are observed although some smearing of the data set is likely due to the analysis of mixed age spots in these demonstrably zoned zircons, as well as the potential for ancient Pb loss, and further obfuscation during recent Pb loss.

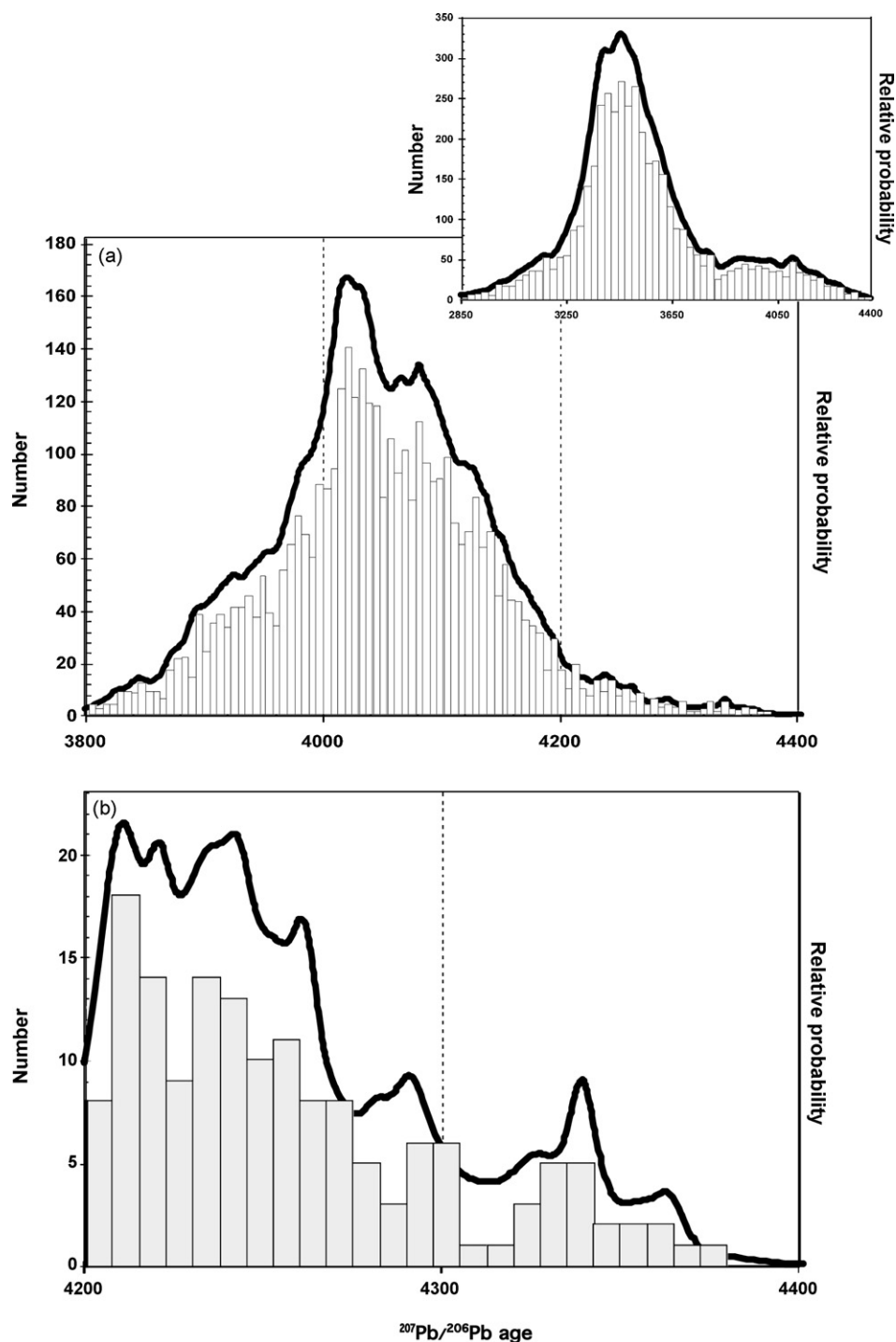


Fig. 10. Histograms and probability-density curves for concordant Jack Hills zircons. (a) Since the criteria for the instigation of a full U–Pb analyses is set by a rapidly determined $^{207}\text{Pb}/^{206}\text{Pb}$ ratio of 0.4 (equivalent to 3940 Ma), the 3.8–3.9 Ga population in this diagram will be seriously underestimated. Inset is the whole population of 4500 rapidly scanned $^{207}\text{Pb}/^{206}\text{Pb}$ ages. (b) Histogram and probability density for the concordant >4.2 Ga zircons. The small peak at 4.35 Ga may be the oldest surviving crustal remnant.

Compston and Pidgeon [2] first considered ancient Pb loss for the distribution of U–Pb data from their Jack Hills zircon population where the oldest 4.26 Ga zircon appears more concordant than the 4.0–4.1 zircons. The lower intercept age of 1900 Ma is potentially a metamorphic age. Ancient Pb loss renders the $^{207}\text{Pb}/^{206}\text{Pb}$ age of any ancient zircons a minimum estimate, and so the younger ages could be the result of originally old zircon being affected by Pb redistribution. However, it is extremely difficult to distinguish between potentially overlapping age zones with recent Pb loss versus ancient Pb loss alone. Where only a few grains are available for

study, it is tempting to fit Pb loss trajectories, however our data set while not ruling out ancient Pb loss, suggests zero age Pb loss to be dominant.

The presence of a distinct age population at 4350 Ma begs the question of where these zircons came from? Of those so far examined, none has returned a single age for the grain rather having a spectrum of events recorded, suggesting a complex history of recycling through several high-temperature events. We conclude therefore, that these grains were themselves an inherited component in the younger granitoids whose eroded

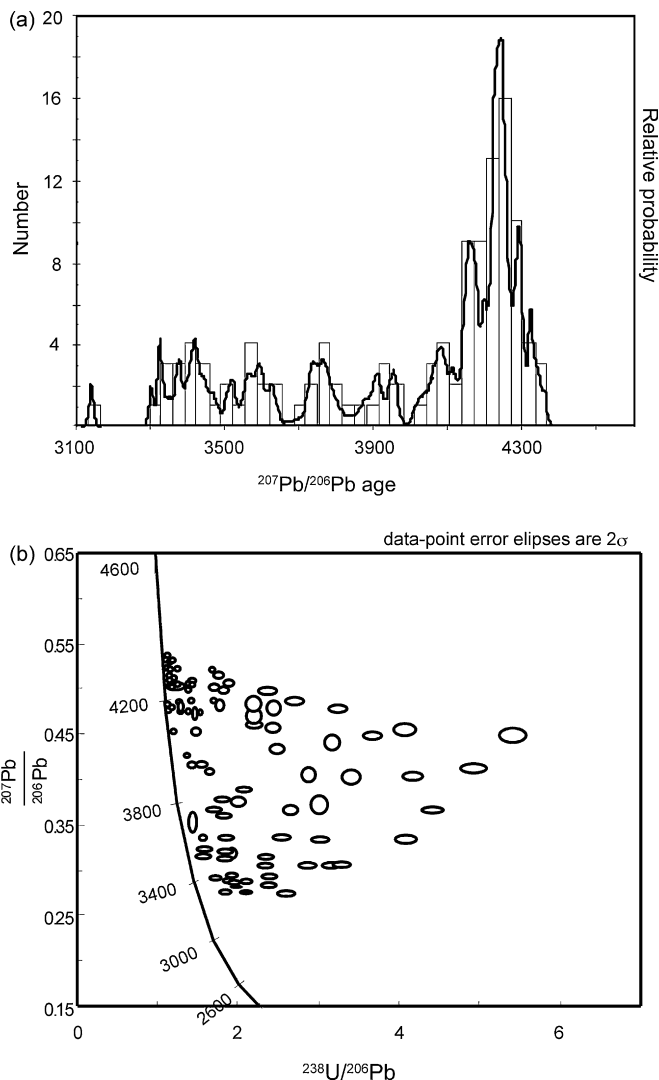


Fig. 11. (a) Histogram of $^{207}\text{Pb}/^{206}\text{Pb}$ ages and probability density plot for a single 4.3 Ga grain (RSES96-15.10). Multiple age peaks attest to the complex history of the grain. (b) Tera-Wasserburg concordia plot showing both ancient (vertical displacement and dominantly recent (horizontal displacement) Pb loss.

remnants were shed into the Jack Hills and Mt Narryer watersheds.

At this stage, further insight into the geological record preserved in the Jack Hills detrital zircon population will not be afforded by amalgamating single point U–Pb analysis of individual grains. There is simply too much potential age range and Pb redistribution available to be able to refine the contributions from each. However, we are now pursuing an approach where the maximum amount of age information can be gleaned from a single grain. The logic is straightforward. If tectonic activity or recycling of the crust was rapid, then a grain from the 4.34 Ga population has the potential to record, as overgrowths or by Pb loss, each of these events. By analyzing multiple spots (possibly hundreds on larger grains) on each individual grain, and comparing these age spectrums, specific tectonic events will emerge as repeated age peaks. Conversely, if each individual records an entirely separate spectrum, then it suggests that crustal recycling was localized and rapid. We show one such provisional data set for sample RSES96-15.10. One hundred and fifteen overlapping spot analyses were obtained from this single grain. On a relative probability plot (Fig. 11a) several discrete peaks can be seen. The oldest component is 4.35 Ga with an overgrowth or Pb

redistribution at 4.25 Ga, a further peak at 4.19 Ga suggests another event, with subsequent events at 4.1, 3.94, 3.8, 3.6 Ga and a continuum (of Pb loss?) around 3.3 Ga, which corresponds to the dominant age group at Jack Hills. Examination of the concordia plot for this grain (Fig. 11b) emphasizes the dominance of recent Pb loss. Interestingly, the 3.94 Ga peak has been identified in depth profiles from four other Jack Hills–Mt Harrier zircons, as a common but volumetrically small outer rind [17]. This they suggest could be a vestige of the late heavy meteorite bombardment at this time. If this is true, the event appears from the evidence of RSES96-15.10 to be no more significant than the several other events this grain has seemingly withstood. Nonetheless, this zircon demonstrates the potential of this technique to unravel the rapidity of crustal processes in the Hadean, even identifying age groups thought accessible only by depth profiling [17]. By comparing similar plots for different grains, it may be possible to build up a picture of the nature, either episodic or continual, of the growth of the earliest fragments of the crust, and will help subsequent studies on these grains to specifically target the most pristine portion of the grain. A statistically reliable view of the Hadean based on multiple analyses of single grains can only be achieved if sufficient “old” grains are found. The search continues.

5. Conclusions

The operation of SHRIMP II in automated multiple-collector mode allows efficient identification of Hadean zircons from the more common Archean contribution. Automated analysis in single-collector mode for SHRIMP I and SHRIMP RG has also been accomplished. From ca. 100,000 zircons analyzed, 5.04% are concordant and Hadean (>4.0 Ga), in both coarse and fine grain-sized zircon fractions. The oldest population of grains we have identified has a mean age of 4.34 ± 0.01 Ga and this likely represents the point at which early continental crust in this region begins to survive geologically reprocessing.

Acknowledgements

This work was supported by ARC Grants DP0342709 and DP0666497. Steve Clement and William Compston were responsible for the original multiple-collector design; Norm Schram designed the electronics. Mount preparation by Sally Mussett and Jane Thorne is gratefully appreciated. We also thank the anonymous reviewer for their insightful comments.

References

- [1] D.O. Froude, T.R. Ireland, P.D. Kinny, I.S. Williams, W. Compston, I.R. Williams, J.S. Meyers, *Nature* 304 (1983) 616–618.
- [2] W. Compston, R.T. Pidgeon, *Nature* 321 (1986) 766–769.
- [3] U. Schärer, C.J. Allègre, *Nature* 315 (1985) 52–55.
- [4] W. Compston, D.O. Froude, T.R. Ireland, P.D. Kinny, I.S. Williams, I.R. Williams, J.S. Meyers, *Nature* 317 (1985) 559–560.
- [5] E.G. Nisbet, N.H. Sleep, *Nature* 409 (2001) 1083–1091.
- [6] I.S. Williams, S.A. Bowring, *Contrib. Mineral. Petrol* 134 (1999) 3–16.
- [7] S.A. Wilde, J.W. Valley, W.H. Peck, C.M. Graham, *Nature* 409 (2001) 175–178.
- [8] T.R. Ireland, F. Wlotzka, *Earth Planet. Sci. Lett.* 109 (1992) 1–10.
- [9] R. Maas, P.D. Kinny, I.S. Williams, D.O. Froude, W. Compston, *Geochim. Cosmochim. Acta* 56 (1992) 1281–1300.
- [10] S.J. Mojzsis, T.M. Harrison, R.T. Pidgeon, *Nature* 409 (2001) 178–180.
- [11] A.N. Halliday, *Nature* 409 (2001) 144–145.
- [12] H. Matsuda, *Int. J. Mass Spectrom. Ion Phys.* 14 (1974) 219–233.
- [13] I.S. Williams, *Rev. Econ. Geol.* 7 (1998) 1–35.
- [14] K.R. Ludwig, *Berkeley Geochronol. Cent. Spec. Publ.* 2 (2001) 1–17.
- [15] L.P. Black, S.L. Kamo, I.S. Williams, R. Mundil, D.W. Davis, R.J. Korsch, C. Foudoulis, *Chem. Geol.* 200 (2003) 171–188.
- [16] J.B. Paces, J.D. Miller, *J. Geophys. Res.* 98 (1993) 13997–14013.
- [17] D. Trail, S.J. Mojzsis, T.M. Harrison, *Geochim. Cosmochim. Acta* 71 (2007) 4044–4065.
- [18] L.P. Black, S.L. Kamo, C.M. Allen, J.N. Aleinikoff, D.W. Davis, R.J. Korsch, I.S. Williams, C. Foudoulis, *Chem. Geol.* 200 (2003) 155–170.